



Norwegian University of
Science and Technology

Muhammad Zohaib Sarwar
Daniel Cantero
Max Hendriks
Mette Rica Geiker

Eurostars project No.: ICD 521
“Intelligent concrete drying”

WP1: Concrete drying model
Task 1.1: Selection of constitutive equation
Task 1.2: Identification of input parameters
Task 1.3: Sensitivity Study

Report

VERSION

1

DATE

18-10-2023

CLIENT(S)

Eurostars-2 joint program

PROJECT NUMBER

No: ICD 521

NUMBER OF PAGES AND ATTACHMENTS

20 pages exclusive list of references (3 pages)

One appendix (3 pages)

Abstract

Based on literature a constitutive equation for drying of concrete and key input parameters were identified (addressing Tasks 1.1 and 1.2 of project ICD 521). The key input parameters are the desorption isotherm and the moisture diffusivity, both in the relevant range of relative humidity (75% to 100% RH). Models describing desorption isotherms and moisture diffusivity of concrete were identified. A modelling framework (script) was prepared to allow for numerical modelling of the drying of a (mature) concrete or self-levelling flooring compound. Finally, a sensitivity study was undertaken (addressing Tasks 1.3 of project ICD 521).

REPORT NUMBER

WP1-A

ISBN

978-82-303-6235-8

CLASSIFICATION

Open

Preface

This report was prepared as part of WP1 “Concrete drying model” of the Eurostars project: “Intelligent concrete drying”, No.: ICD 521 with the project time 1/9-2022 to 31/8-2024.

The overall objective of the project is to develop a solution consisting of sensors and software that can save 25-30% of the energy consumed for drying concrete on a job site. In the Nordic countries alone, the potential is estimated to more than 212.000 tons/CO₂ per year. The solution is additionally expected to save time and money at the same time. During the project, a suitable mathematical description of concrete drying will be identified and combined with the latest within data modelling. A software platform will be developed, and tests will be carried out on several jobsites in Denmark and Norway.

As the lead partner of WP1 “Concrete drying model”, NTNU carries out the following tasks:

- Task 1.1 “Selection of constitutive equation”
- Task 1.2 “Identification of input parameters”
- Task 1.3 “Sensitivity study”

In the proposal, these tasks were suggested undertaken through combined literature study and experimental testing (former Task 1.4 “Moisture profiles”). However, based on the researcher’s extensive competence in numerical modelling it was decided not to undertake experimental studies in WP1, but establish a numerical model, use input parameters from literature and supplier, and perform the sensitivity study through numerical simulations.

List of symbols and abbreviations

α	Degree of hydration	-
$\alpha_h, \beta_h, \gamma_h$	Parameters for Eq. 15	-
C	Amount of cement	kg
C_t	Type of cement	-
D_h	Moisture diffusivity	m ² /s
ε_{tot}	Total (suction) porosity of cement paste	kg/m ³
h	Internal relative humidity (RH)	Pa/Pa
k_{wg}	Maximum amount of water in the gel pores per mass of cement	kg/kg
L	Depth of slab	m
OPC	Ordinary Portland Cement	-
SLC	Self-levelling flooring compounds	-
RH	Relative humidity	%
v_s	Vapour content at saturation	kg/m ³
w/c (or w/c-ratio)	Water-to-cement ratio	-
w_{cap}	Capillary water	kg/m ³
w_{cs}	Change in evaporable water due to chemical shrinkage	kg/m ³
w_e	Evaporable (physically bound and free) water	kg/m ³
$w_{e,sat}$	Evaporable (physically bound and free) water at saturation	kg/m ³
w_{gel}	Gel (physically bound) water	kg/m ³
w_n	Non-evaporable (chemically bound) water	kg/m ³
w_0	Total amount of (mixing) water	kg/m ³
δ_{tot}	Total moisture transport coefficient	m ² /s
$\frac{\partial w_e}{\partial h}$	Slope of sorption isotherm	kg/m ³

Acknowledgements

EU funding through the Eurostars project: “Intelligent concrete drying”, No.: ICD 521 and the collaboration with the partners (Maturix/Sensohive (Denmark) University of Southern Denmark (Denmark), Betonmast Buskerud-Vestfold (Norway)) are greatly acknowledged.

Table of Contents

<i>Preface</i>	II
<i>List of symbols and abbreviations</i>	III
<i>Acknowledgements</i>	III
1. Introduction	1
2. Moisture transport models	2
3. Input parameters	3
3.1 <i>Water vapour desorption isotherm</i>	4
3.1.1 Moisture in cementitious materials	4
3.1.2 Modelling water vapour desorption isotherms	6
3.1.3 Influence of temperature on sorption isotherms	7
3.1.4 Water vapour sorption isotherms of self-levelling flooring compound	8
3.2 <i>Moisture transport</i>	11
3.2.1 <i>Modelling moisture diffusivity in concrete</i>	12
3.2.2 Total moisture transport coefficient of self-levelling flooring compound	14
4. Numerical modelling of drying of cementitious material	16
4.1 <i>Modelling framework</i>	16
4.2 <i>Case study</i>	17
5. Sensitivity study	18
6. Conclusion	19
References	21
Appendix	24

1. Introduction

The “Intelligent concrete drying” project (ICD 521) was motivated by general contractors pushing for a more sustainable future. In the Nordic countries, all general contractors are expected to build more sustainably. The drying of concrete consumes 50-70% of all energy on a typical building job site, and studies have shown that if optimised it could be halved (ICD 521). The ICD 521 project aims at making concrete drying more efficient and at facilitating data-driven decisions, resulting in cost, time, and CO₂ savings.

For flooring, the structural concrete in residential and office buildings is typically covered with a self-levelling flooring compound (SLC) before overlaying with a surface covering like PVC flooring or wooden parquet. Typically, a dry SLC is mixed with water to achieve the required workability for self-levelling during construction. Part of the mixing water reacts with the binder, whereas the remaining moisture content (evaporable water, see Section 3) in the hardened SLC must be reduced to prevent damage to the overlay and the indoor climate.

1.1 Objectives and content

This report addresses Task 1.1” Selection of constitutive equation”, Task 1.2 “Identification of input parameters” and Task 1.3 “Sensitivity study” of the ICD 521 project.

Based on literature, a constitutive equation for drying of concrete and key input parameters are identified in Section 2. Models describing the key input parameters (desorption isotherms and moisture diffusivity of concrete) are identified in Section 3. Considering the cases provided by the industrial partners, the key material is not necessarily structural concrete, but alternatively a self-levelling flooring compound being applied late in the building process, input data for such materials was identified and compared to the models for concrete. Finally, a modelling framework (script) was prepared to allow for numerical modelling of the drying of a (mature) concrete or self-levelling flooring compound, and the script was tested towards data from commercial software in Section 4. The numerical modelling approach for drying utilizes a single partial differential equation of the diffusion process and assumes the material to be well hydrated, i.e., not undergoing further hydration causing microstructural changes and continued self-desiccation. Section 4 also summarizes key assumptions. Section 5 provide the result of sensitivity study.

2. Moisture transport models

In its simplest form, the drying process can be described by a second-order differential equation of moisture diffusion (Bažant & Najjar 1972). However, the coefficients in this equation (moisture diffusivity and moisture capacity) are highly dependent on concrete properties and moisture state making the problem nonlinear (see Section 3).

Drying is a diffusion process, and the modelling of drying is based on Fick's second law. There are two primary driving forces considered in modelling moisture diffusion problems:

1. Gradient of evaporable water as the driving force
2. Gradient of internal relative humidity (RH) as the driving force.

Both approaches involve formulating the diffusion coefficient in terms of either the water content or the RH of the concrete. The RH-based formulation is generally considered more convenient than the water content-based formulation. The main disadvantage of the water content-based approach is the difficulty in expressing boundary conditions in terms of water content.

The drying process of concrete is typically represented by a second-order parabolic differential equation (Bažant & Najjar 1972; Xi et al. 1994a, b), with the relative humidity as an independent variable:

$$\frac{\partial w_e}{\partial h} \frac{\partial h}{\partial t} = \frac{\partial}{\partial x} \left[D_h \frac{\partial h}{\partial x} \right] \quad \text{Eq. 1}$$

where u is the moisture content in kg/kg, h is the internal relative humidity in Pa/Pa, $\frac{\partial w_e}{\partial h}$ is the slope of the desorption isotherm. D_h is the moisture diffusivity in m²/s, t is the time in seconds, and x is the space in meter.

To solve the differential equation (Eq. 1), it is necessary to determine two key parameters that, among others, depend on the concrete composition and degree of hydration:

- Water vapour desorption isotherm
- Moisture diffusivity.

In addition, the impact of self-desiccation on the moisture state during drying needs to be known. These parameters can either be obtained experimentally or theoretically. Models for the development of self-desiccation were e.g., proposed by Mjörnell (1997), Persson (1997) and Oh & Cha (2003).

Features of selected models for water vapour transport in cementitious materials are summarized in Table 1 and briefly discussed below. Two of the mentioned models include transport of heat (Künzel 1995) and (Sekki et al. 2017). Reactive mass transport models (see e.g., (Sharmilan et al. 2023) describe multi-species transport and interaction between the solids and the pore liquid. These models are considered too elaborate for the present application and thus not covered here.

Bažant & Najjar's (1972) widely cited physical model, which relies on a nonlinear diffusion equation, improved upon previous linear models but depends on empirical coefficients and a linear sorption isotherm. (Parrott 1988) developed an empirical model where the moisture content depended on water-to-cement ratio (w/c-ratio) and the ambient (external) relative humidity. (Xi et al. 1994a, b) modified Bažant and Najjar's model by using the Brunauer-Skalny-Bodor (BSB) sorption isotherm model and defining moisture diffusivity independent of the w/c-ratio.

Künzel (1995) proposed a physically based model for simultaneous heat and moisture transport. Mjörnell (1997) proposed a self-desiccation model using a sorption isotherm and accounting for hydration, concrete composition, and internal relative humidity. Persson (1997) created an empirical model for concrete drying

that included self-desiccation and expressed internal relative humidity in terms of the w/c-ratio, curing type, and time. Breugel & Koender (2001) developed a physical model of moisture transport based on concrete's microstructure, differentiating between bulk paste and interfacial paste. Pel (2002) offered an analytical solution for a nonlinear drying problem, resulting in a constant drying front speed entering the material, consistent with experimental observations.

Oh & Cha (2003) devised a nonlinear empirical model for moisture loss due to self-desiccation concerning the degree of hydration and w/c-ratio. Baroghel Bouny (2007a, b) conducted extensive experiments to study the impact of w/c-ratio on moisture properties, microstructural features, and transport properties in various normal and high-performance hardened cement pastes and concretes, assessing moisture profiles through gamma-ray attenuation measurements. Sekki et al. (2017) developed a numerical simulation model to study the drying of concrete slabs. In this model, coupled equations of heat and moisture transport in porous materials, including the hydration phenomenon, were solved using the finite element method.

For the present application Eq. 1 describing the drying process of concrete at constant temperature will be used. Models for water vapour isotherms, self-desiccation, and moisture diffusivity are identified in Section 3.

Table 1: Features of selected models for water vapour transport in cementitious materials.

Reference	Transport of		Impact of self-desiccation	Parameters	
	Moisture	Heat		Physical	Empirical
(Bažant & Najjar 1972)	X				X
(Parrott 1988)	X				X
(Xi et al. 1994a, b)	X			X (BSB sorption isotherm)	
(Künzel 1995)	X	X		X	
(Mjörnell 1997)	X		X		X
(Persson 1997)	X		X		X
(Breugel & Koender 2001)	X			X (microstructure development)	
(Pel 2002)	X			X	
(Oh & Cha 2003)	X		X		X
(Baroghel Bouny 2007a, b)	X				X
(Sekki et al. 2017)	X	X			X

3. Input parameters

Models for water vapour isotherms, self-desiccation, and moisture diffusivity are identified in this section. In addition, literature data for self-levelling flooring compounds (SLCs) is provided. These data are considered valuable for the present application as the models available in the literature are based on experimental work on ordinary Portland cement (OPC), and detailed informed mix composition of the SLCs typically not are shared by producers. In addition, it should be noted that that in addition to mix composition and degree of reaction, mixing and curing affects the final microstructure and thus transport properties of cementitious materials (Hooton et al. 2002; Geiker et al. 2007; Geiker 2023). It is therefore of importance to access to which extend literature data is applicable for a given case.

3.1 Water vapour desorption isotherm

3.1.1 Moisture in cementitious materials

The moisture state of cementitious materials changes with time. Initially, when cement and other binders are mixed with water an aqueous suspension is formed. Rapidly, the binder starts to dissolve, and the mixing water becomes an aqueous solution of ionic species causing a small reduction in relative humidity (RH) (approximately 2%). When the ionic concentration is sufficiently high, hydration products start to precipitate. Gradually, more and more hydration products are formed on the expense of the unreacted binder and free water. During hydration, water becomes chemically bound in the hydration products and physically bound, either adsorbed on internal surfaces or capillary absorbed in pores. At a w/c-ratio below a composition dependent threshold, for Portland cement typically 0.4 by weight of cement, no free water is left at full hydration. The chemical binding of the water reduces its specific volume, which results in so-called chemical shrinkage. Initially, when the matrix is plastic, chemical shrinkage is accompanied by bulk shrinkage (autogenous deformation), but after the cementitious material has obtained a rigid microstructure, chemical shrinkage results in internal drying. The chemical shrinkage will only manifest itself in a RH reduction (so-called self-desiccation) if the menisci being set up in the pores due to the internal drying are sufficiently small. If self-desiccation leads to high internal stresses compared to the materials capacity, further autogenous deformation will occur. In summary with relation to drying: the RH in a saturated cementitious material is reduced by approximately 2% due to high ionic concentration of the pore solution. The chemical and physical binding of water reduce the free water content and chemical shrinkage may lead to self-desiccation/reduced RH, depending on the binder and mix composition, and possible access to extra curing water.

The hydrated cementitious material contains pores in a range from a few nano-meter-sized inter-layer (radius ≈ 1 nm) and gel pores (radius ≈ 3 nm) to larger inter-hydrate (radius ≈ 10 nm) and larger capillary pores (radius > 10 nm) (Muller et al. 2013). If sealed cured, chemical shrinkage leads to part of these capillary pores becoming empty (so-called contraction pores). The pore structure is complicated and depends on both the composition and the curing conditions (temperature and RH).

The evaporable water, which covers the physically bound and free water, is typically characterized by isotherms describing the relation between water content (or degree of saturation) and RH or pore water pressure at a constant temperature, see Figure 1. Moisture sorption isotherms¹ cover the so-called hygroscopic range from 0 to 98% RH where water is physically bound (adsorbed and capillary absorbed), whereas suction curves² include both physically bound and free water (Nilsson 2018).

When in contact with the surroundings, the moisture in the cementitious materials will equilibrate with the boundary conditions. Due to the complicated pore structure, the water content at a given RH depends on the moisture history, especially if drying (desorption branch) or adsorbing moisture (adsorption branch), see Figure 2. The moisture capacity, the ability of the material to bind or loose moisture when RH changes, is determined from the slope of the sorption isotherm.

¹ Moisture sorption isotherm: the relationship, at a certain temperature, between the moisture content of the material and the relative humidity (Muller et al. 2013)

² Suction curve: the relationship, at a certain temperature, between the moisture content of the material and the pore water pressure (Muller et al. 2013)

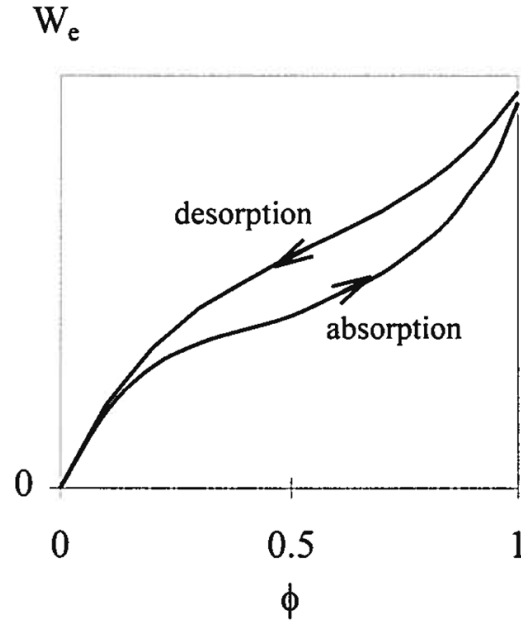


Figure 1 - Schematic absorption and desorption isotherms of concrete. Copy from Mjörnell (1997), who used capital letters for symbols.

If cured sealed (i.e., without access to extra water), the evaporable water becomes

$$w_e = w_0 - w_n \quad \text{Eq. 2}$$

where w_e is the evaporable (physically bound and free) water, w_0 is the total amount of (mixing) water, and w_n is the non-evaporable (chemically bound) water (all in mass).

Due to chemical shrinkage part of the porosity becomes void. If cured saturated, the evaporable water would be

$$w_{e,sat} = w_0 - w_n + w_{cs} \quad \text{Eq. 3}$$

where $w_{e,sat}$ is the evaporable (physically bound and free) water in a fully saturated paste, and w_{cs} is the imbibed (additional) water due to chemical shrinkage.

The total (suction) porosity of cement paste (ϵ_{tot}) can be determined using the so-called Powers' model (see e.g., (Brouwers 2004)):

$$\epsilon_{tot} = \frac{\frac{w}{c} - (1 - 0.254)w_n}{\frac{1}{3.12} + \frac{w}{c}} \quad \text{Eq. 4}$$

where w/c is the water-to-cement ratio, and w_n is the non-evaporable (chemically bound) water, (all in mass). If rearranged and assuming fully saturated eq. 3 becomes

$$w_{e,sat} = w_0 - 0.75w_n \quad \text{Eq. 5}$$

where $w_{e,sat}$ is the evaporable (physically bound and free) water, and w_0 is the total amount of (mixing) water, (all in mass). The use of eq. 5 is illustrated in Figure 2.

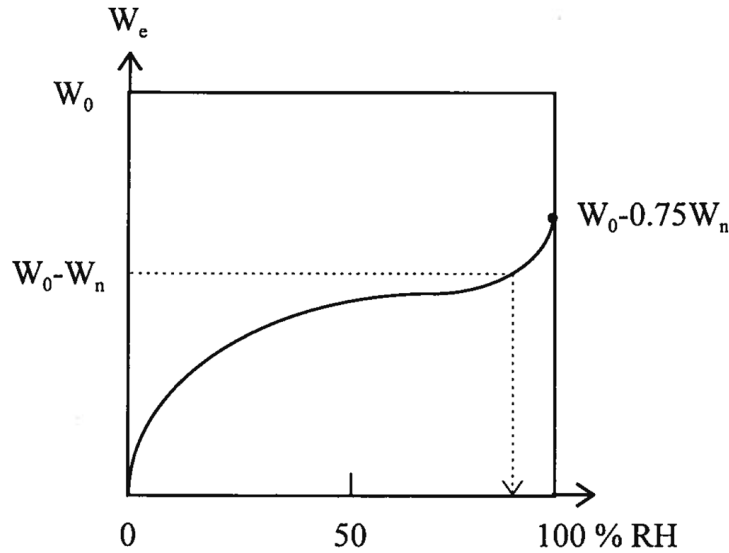


Figure 2 – Schematic relation between evaporable water content and RH. w_e : evaporable water, w_n : non-evaporable water, w_0 : initial water content. Copy from Mjörnell (1997), who used capital letters for symbols.

Both values of non-evaporable water and chemical shrinkage depends on the composition of the binder, degree of reaction and the curing temperature, see e.g., (Geiker 2016; Lothenbach et al. 2016). Knowing the binder composition and the degree of reaction, the values can be calculated using thermodynamic modelling. As a first approximation typical values from Powers' work³ might be used:

$$W_n = 0.23 \text{ g/g cement reacted} \quad \text{Eq. 6}$$

$$W_{CS} = 0.064 \text{ g/g cement reacted} \quad \text{Eq. 7}$$

Eq.7 is in the modelling approach used for estimation of self-desiccation, i.e., the reduction in non-evaporable water due to chemical shrinkage.

3.1.2 Modelling water vapour desorption isotherms

Following the arguments by Mjörnell (1997), the amount of evaporable water (w_e) can be determined from the sum of the gel water (w_{gel}) and the capillary water (w_{cap}), which both depend on the RH (h) and the degree of hydration (α):

$$w_e(h, \alpha) = w_{gel}(h, \alpha) + w_{cap}(h, \alpha) \quad \text{Eq. 8}$$

Where for Portland cement paste

$$w_{gel}(h, \alpha) = w_{gel} \cdot \left(1 - \frac{1}{e^{(b-a \cdot 10) \cdot h}}\right) \quad \text{Eq. 9}$$

$$w_{gel} = k_{wg} \cdot \alpha \cdot C \quad \text{Eq. 10}$$

$$w_{cap}(h, \alpha) = w_{cap} \cdot (e^{(b-a \cdot 10) \cdot h} - 1) \quad \text{Eq. 11}$$

³ American Portland cements around 1950. See e.g., (Brouwers 2004), for an extensive discussion of Powers and colleagues.

$$W_{cap} = \frac{w_{e_sat} - w_{gel} \cdot \left(1 - \frac{1}{e^{(b-a \cdot 10) \cdot h}}\right)}{e^{(b-a \cdot 10) \cdot h} - 1} \quad \text{Eq. 12}$$

k_{wg} represents the maximum amount of water in the gel pores plus the water in the contraction pores per mass of reacted cement (typically 0.21 according to Mjörnell (1997)), and C is the amount of cement. k_{wg} and b are estimated by fitting calculated desorption sorption isotherms to measured desorption isotherms.

Figure 3 illustrates the influence of degree of hydration (age) on the water vapour desorption moisture content computed by using Eq. 8. It can be observed that the shape of water vapour desorption isotherm remains same, and that increasing degree of hydration causes an increased water retention at low relative humidities and a reduced total porosity.

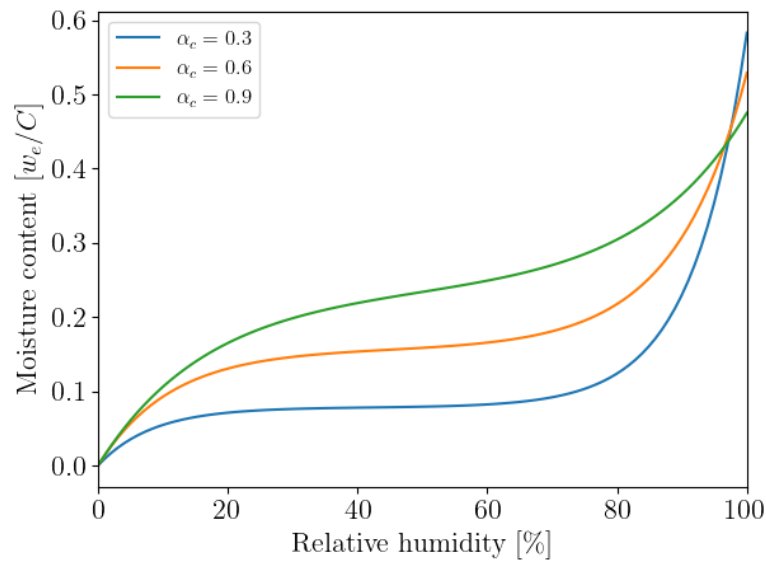


Figure 3: Influence of degree of hydration (age) on water vapour desorption isotherms for pastes with $w/c=0.7$ and OPC Slite cement. Data from (Mjörnell 1997).

3.1.3 Influence of temperature on sorption isotherms

Water vapour sorption isotherms of cementitious materials shifts to the right with increasing temperature at a constant moisture content. Radjy et al. (2003) discussed the effect of temperature on water vapour sorption isotherms for cement paste and reported data. The observed a common trend of an increased RH change when at drying from saturation until the RH-midrange followed by a reduction at further drying, see Figure 4. The magnitude of the effect is about 0.3-0.4% RH/°C at 75-85% RH.

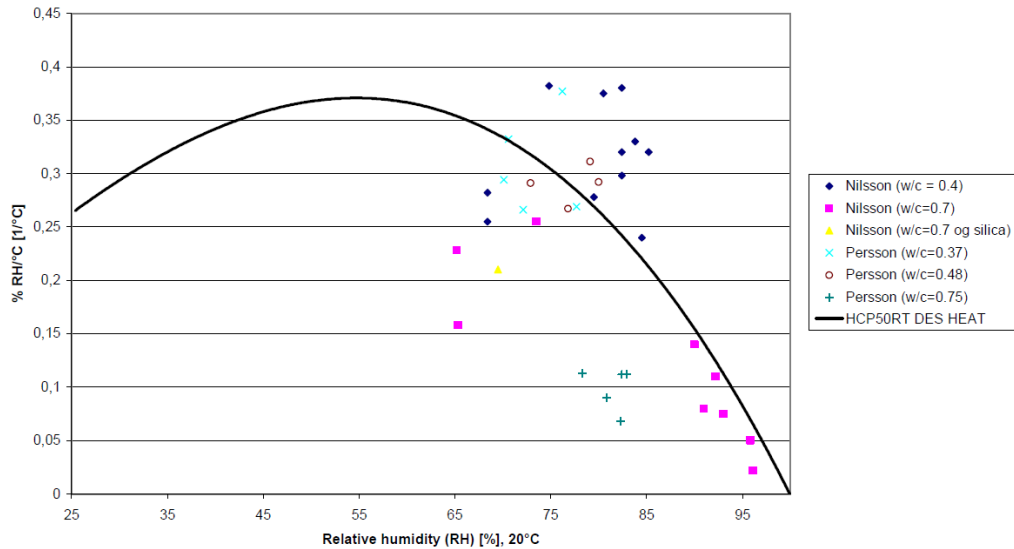


Figure 4 - Temperature effect on RH change at given constant moisture content for cement paste. Copy from (Radjy et al. 2003).

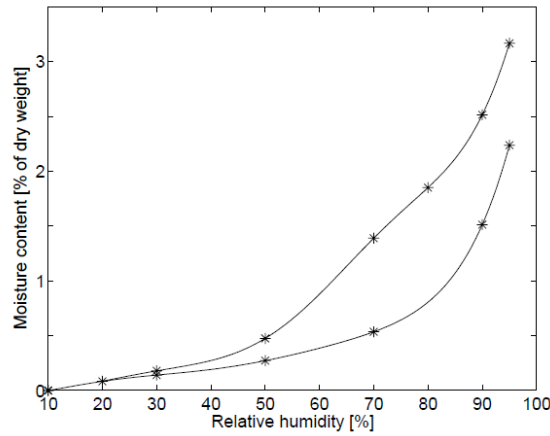
3.1.4 Water vapour sorption isotherms of self-levelling flooring compound

(Anderberg and Wadsö 2004), in addition to determination of total moisture transport coefficient, experimentally determined the water vapour sorption isotherms of self-levelling flooring compounds (SLC), using three different commercial products, A: a normal SLC ($w/c \approx 1.0$) typically used for non-industrial structures, B: a rapid-drying SLC with higher self-desiccation ($w/c \approx 0.7$), and C: a SLC for industrial floors ($w/c \approx 0.6$). The products were mixed according to the manufacturer's guidelines, stored for 24 hours at 20°C and 50% RH, and subsequently in sealed in glass jars with small amounts of excess water to keep 100% RH. Measurements were undertaken after 12 months. A sorption balance (DVS 1000, Surface Measurements Systems, London, UK) was used to determine water vapour sorption isotherms and scanning curves. The sorption isotherms were presented as moisture content (relative to mass at 10% RH, here called dry weight) as a function of RH. The measured data are shown in Figure 5 (note the differences in axes).

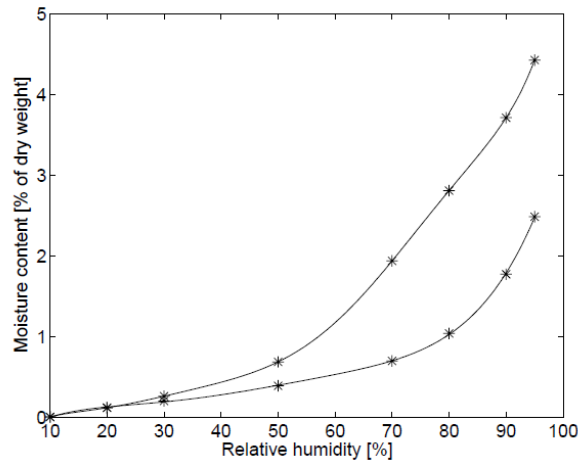
Figure 6 provides water vapour sorption isotherms measured after one, three, and twelve months. Limited further moisture retention from one to twelve months is observed, which indicates that the microstructure was well developed already after one month. The impact of w/c -ratio on water vapour sorption isotherms is illustrated in Figure 7, showing data for mixing water variations comparable to the variation used in Table 3.

In addition to the composition, the moisture history, and the environmental exposure (here temperature) affect the water vapor sorption isotherm. In the range 75-100% RH, the adsorption isotherms are steeper than the desorption isotherms (see Figure 5 and 6). Figure 8 shows a reduced moisture capacity in the hygroscopic range covered at increased temperature, but also almost parallel desorption curves in the interval 70% to 95% RH.

SLC-A



SLC-B



SLC-C

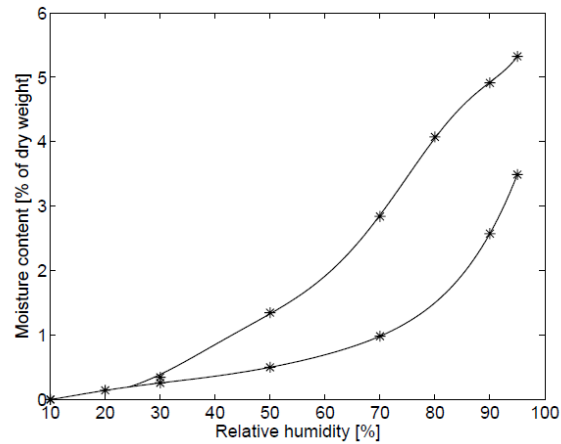


Figure 5: Water vapour sorption isotherms for self-levelling flooring compounds SLC-A, SLC-B, and SLC-C (see text for further details). The stars indicate experimental data. The lines were provided by the original authors and are only for visual guidance and does not represent modelling. The upper curves are desorption isotherms, the lower curves are adsorption isotherms. Note the differences in the vertical axes. Data from (Anderberg & Wadsö 2004).

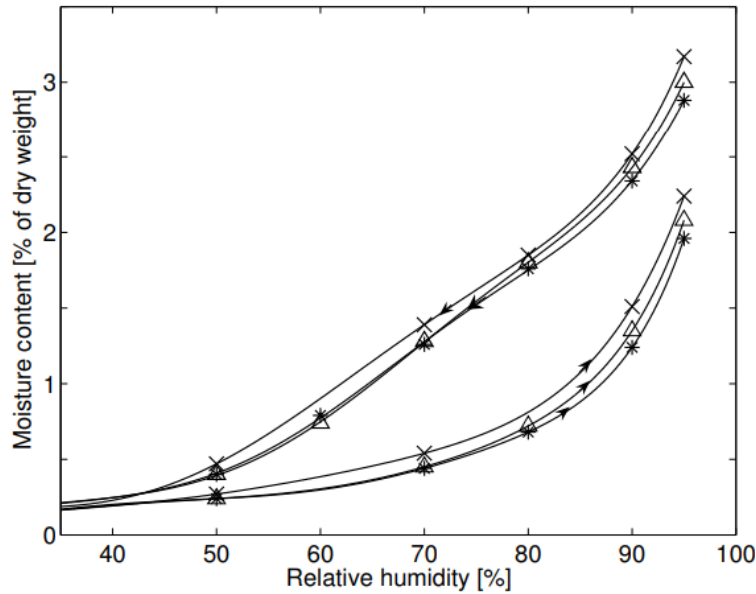


Figure 6: Water vapour sorption isotherm of the self-levelling flooring compound SLC-A at 1 month (stars), 3 months (triangles) and 12 months (x-marks) of age. The upper curves are desorption isotherms, the lower curves are adsorption isotherms. Measurement values below 40% RH showed only small differences and were not included. The lines were provided by the original authors and are only for visual guidance and does not represent modelling. Data from (Anderberg & Wadsö 2004).

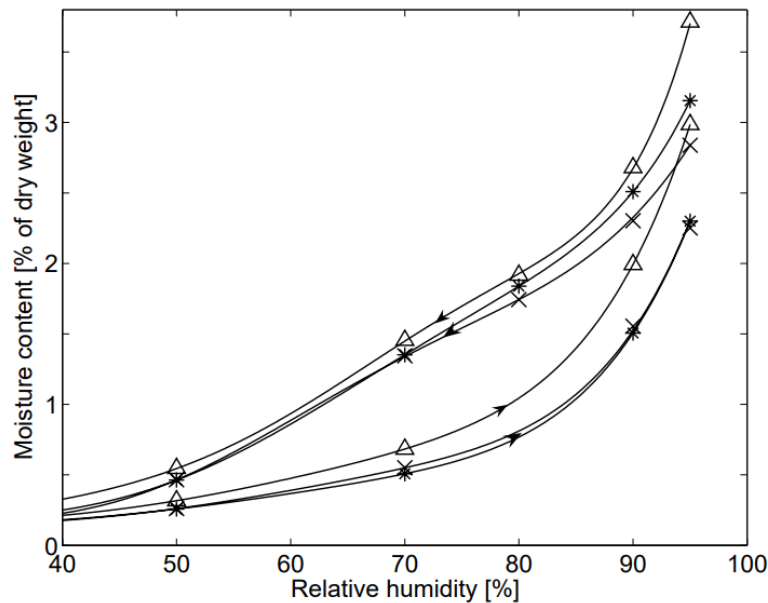


Figure 7: Water vapour sorption isotherms of the self-levelling flooring compound SLC-A cast with $w/c \approx 1.0$ (stars), 10% more mixing water than recommended (x-marks), and 20% less mixing water than recommended (triangles). The upper curves are desorption isotherms, the lower curves are adsorption isotherms. Measurement values below 40% RH showed only small differences and were not included. The lines were provided by the original authors and are only for visual guidance and does not represent modelling. Data from (Anderberg & Wadsö 2004).

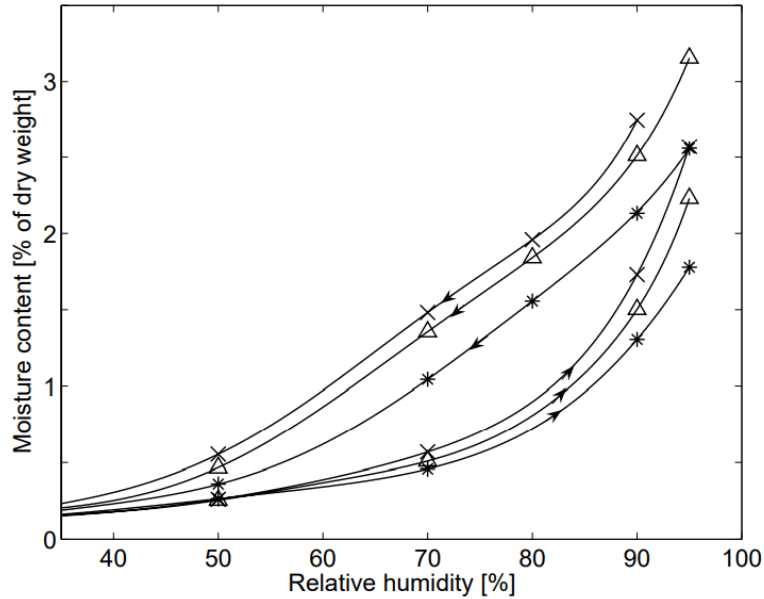


Figure 8: Water vapour sorption isotherms of the self-levelling flooring compound SLC-A at 10°C (x), 20°C (triangles) and 40°C (stars). The upper curves are desorption isotherms, the lower curves are adsorption isotherms. Measurement values below 40% RH showed only small differences and were not included. The lines were provided by the original authors and are only for visual guidance and does not represent modelling. Data from (Anderberg & Wadsö 2004).

3.2 Moisture transport

Various methodologies exist to assess moisture transport properties. The "cup method", a steady-state approach, is among the most prevalent. In this technique, a sizable segment of the material overlays a cup filled either with water or a saturated salt solution, maintaining a designated RH on one side of the material. The cup (and material) is subsequently housed within a controlled RH environment. The cup's weight is continually monitored until a consistent moisture transition through the material is achieved. A notable limitation of this technique is its time-consuming nature, particularly for dense materials like concrete with low w/c-ratio. Nonetheless, a distinct advantage is the straightforwardness in calculating the total moisture transport coefficients (δ_{tot}).

Alternative strategies involve drying specimens with an initial uniform moisture state, all the while tracking the weight decrement. Termed the non-steady method, this approach witnesses variable moisture flow throughout the experiment. From the solutions derived from the mass-balance equation, a transport coefficient, the moisture diffusivity (D_h), can then be deduced.

$$\frac{\partial w_e}{\partial t} = \frac{\partial}{\partial x} \cdot D_h \cdot \frac{\partial w_e}{\partial x} \quad \text{Eq. 13}$$

To facilitate a comparison of the total moisture transport coefficient and moisture diffusivity, Mjörnell (1997) provided the following expression:

$$\delta_{tot} = D_h \times \frac{\partial w_e}{\partial h} \times \frac{1}{v_s} \quad \text{Eq. 14}$$

Where v_s is water vapour content in air at temperature 20°C. The moisture capacity in concrete $\frac{\partial w_e}{\partial h}$ is obtained from the desorption isotherm.

3.2.1 Modelling moisture diffusivity in concrete

For numerical modelling mathematical expression is required for the moisture diffusivity. Table 2 summarises selected models for moisture diffusivity of concrete from the literature with respect to their dependencies on material properties and exposure. Table 3 summarizes experimental data used for development and verification of the models. The models proposed by Xin (1995) and Parrot (1998) are not considered further due to their limited applicability to very specific case studies.

Table 2: Input parameters used in models for concrete moisture diffusivity.

Reference	Material properties			Exposure		Comments (see Table 2 for limitations of experimental data)
	α	w/c	C_t	RH	T	
(Bazant & Najjar 1972)		x	x	x	x	Empirical and experimentally verified model
(Xin 1995)		x	x	x	x	Inverse analysis
(Parrot 1998)		x	x	x		Empirical
(Xi et al. 1994a, b)	x	x	x	x	x	Empirical and experimentally verified model

a: Degree of hydration C_t : Type of cement

Table 3: Experimental data used for development and verification of models for concrete moisture diffusivity.

Reference	Material		Comments
	w/c	Type of cement	
(Bazant & Najjar 1972)	0.3 to 0.7	OPC	w/c range is not well defined however studies show that for low w/c ratio formula didn't show satisfactory performance (Xi et al. 1994a, b), (Xin 1995), (Künzel 1995))
(Xi et al. 1994a, b)	0.45 to 0.7	OPC	In previous studies (Vinkler et al. 2016) model is widely applied for estimation and calculation of moisture diffusivity

OPC: Ordinary Portland cement

The moisture diffusivity as a function of RH modelled using the expressions proposed by (Bazant and Najjar 1972) and (Xi et al. 1994a, b) (see Eq. 15 and 16) is illustrated in Figure 9. The moisture diffusivity values vary significantly between the models in the relevant range RH range. The primary reason for this variation can be attributed to the different material properties of the concrete used to determine the parameters of the equations. (Xi et al. 1994a, b)

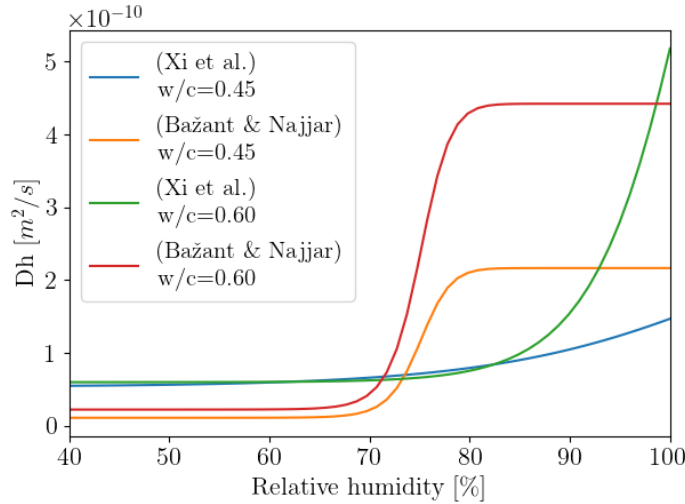


Figure 9: Comparison of moisture diffusivity (D_h) as a function of RH according to (Xi et al. 1994) and (Bazant & Najjar 1972) for OPC concrete with w/c-ratio 0.45 and 0.60

In the present work, the expression proposed by Xi et al. (1994a, b) will be used as more correctly resembles experimental data (see Figure 9). The only input parameters the w/c-ratio, as shown in Eq.15 and Eq.16.

$$D_h = \alpha_h + \beta_h \left[1 - \exp(-10^{\gamma_h(h-1)} \ln 2) \right] \quad \text{Eq. 15}$$

Where the parameters α_h , β_h , γ_h are:

$$\alpha_h = 1,05 - 3,8 \frac{w}{c} + 3,56 \left(\frac{w}{c} \right)^2$$

$$\beta_h = -14,4 + 50,4 \frac{w}{c} - 41,8 \left(\frac{w}{c} \right)^2 \quad \text{Eq. 16a-c}$$

$$\gamma_h = 31,3 - 136 \frac{w}{c} + 162 \left(\frac{w}{c} \right)^2$$

Figure 10 displays the moisture diffusivity values for selected w/c-ratios. The trend of increasing moisture diffusivity with increasing w/c-ratio is attributed to the changes in pore structure. At lower humidity levels transport occurs solely as vapour diffusion, whereas capillary condensation leads to an increased diffusivity at high humidity levels.

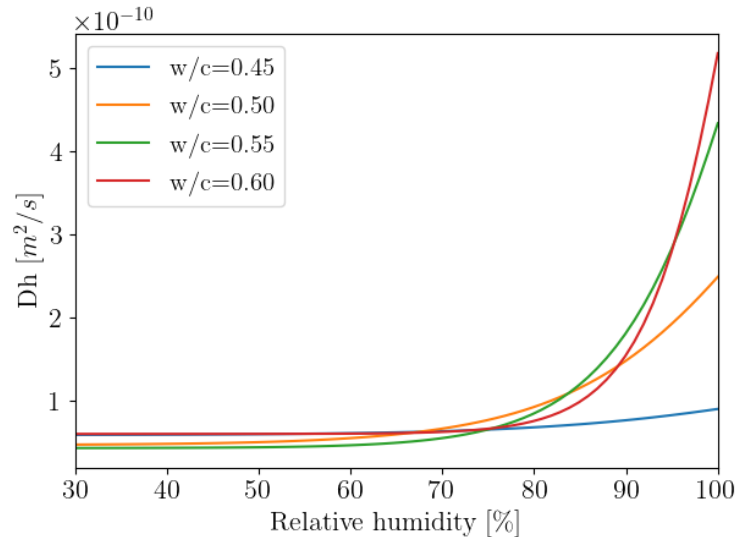


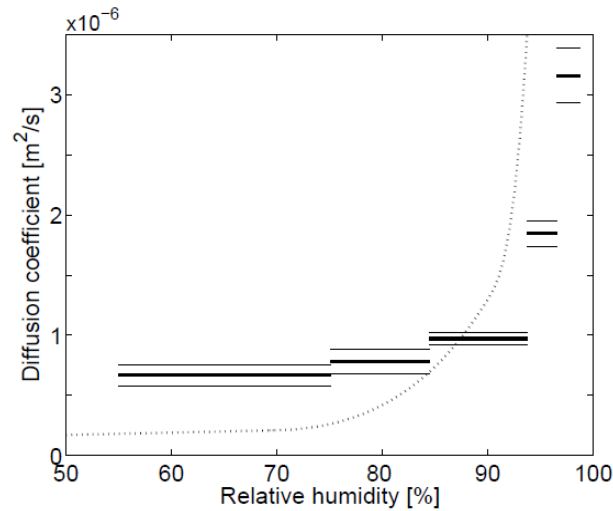
Figure 10: Influence of w/c-ratio on the moisture diffusivity for concrete according to Eq. 14 & 15 (Xi et al. 1994a, b).

3.2.2 Total moisture transport coefficient of self-levelling flooring compound

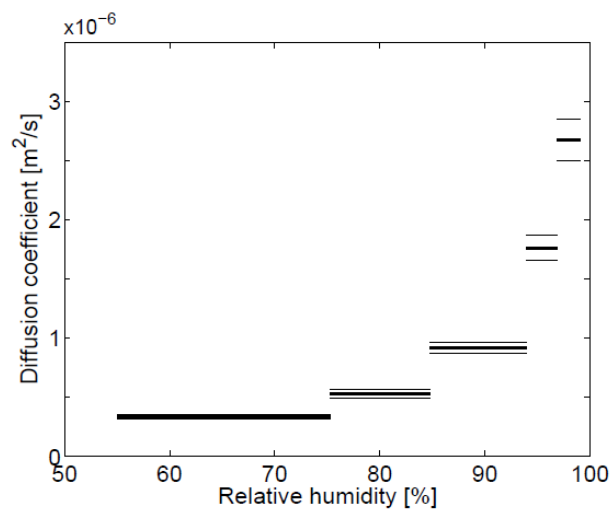
Anderberg and Wadsö (2004) experimentally determined the total moisture transport coefficient of three different commercial products self-levelling flooring compounds (SLCs): SLC-A ($w/c \approx 1.0$) typically used for non-industrial structures; SLC-B, a rapid-drying SLC with higher self-desiccation ($w/c \approx 0.7$); and SLC-C used for industrial floors ($w/c \approx 0.6$). The products were mixed according to the manufacturer's guidelines, stored for 24 hours at 20°C and 50% RH and subsequently in sealed plastic bags. Measurements were undertaken after 2-6 months. The measured data are shown in Figure 4. The impact of w/c-ratio is illustrated when comparing Figures 11a and 11b; as expected a reduced rate of transport is observed for the lower w/c-ratio. (Anderberg & Wadsö 2004) compared the measured total moisture transport coefficient of the SLCs and a selected concrete (w/c-ratio 0.7), see Figure 11a, dotted line,) and found that the SLC has comparable (SLC-B) or a slightly higher (SLC-A) total moisture transport coefficient below 80% RH, but has a lower total moisture transport coefficient at higher RH.

The influence of variations in mixing water is illustrated in Table 4. The observed impact of w/c-ratio is aligned with to the impact w/c-ratio on concrete (see Figure 10) In addition to the composition, the environmental exposure and the moisture history affects the moisture transport.

SLC-A



SLC-B



SLC-C

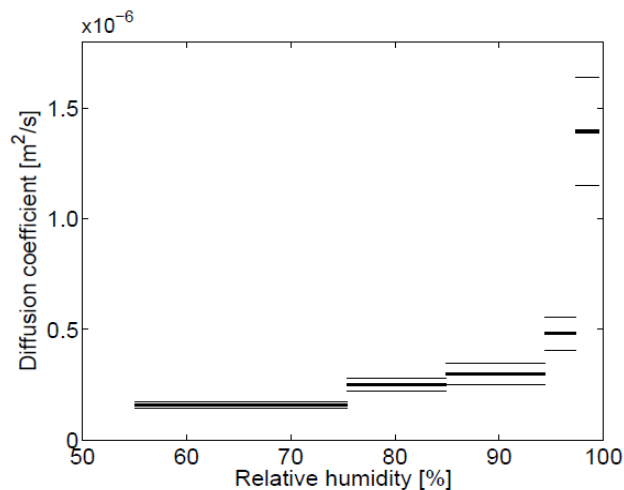


Figure 11: Total moisture transport coefficients for self-levelling flooring compounds (SLCs). SLC-A: a normal SLC ($w/c \approx 1.0$) typically used for non-industrial structures; SLC-B: a rapid-drying SLC with higher self-desiccation ($w/c \approx 0.7$), and SLC-C: a SLC for industrial floors ($w/c \approx 0.6$). The thick and the fine lines indicate mean and standard deviation. The dotted line in Figure 11a shows data for concrete. Copy from (Anderberg & Wadsö 2004), note that Anderberg and Wadsö are using different nomenclature from one used in this report (“Diffusion coefficient” versus “Total moisture transport coefficient” here).

Table 4: Total moisture transport coefficients (mean and standard deviation) for mixes of self-levelling flooring compound (SLC-A, age more than two months) made with different amounts of mixing water. Reference: w/c \approx 1.0). Four replicates were measured of each sample. Data from (Anderberg & Wadsö 2004).

Mix	RH-interval (%)	Total moisture transport coefficients ($10^{-6} m^2/s$)
Reference	55-85.1	0.70 \pm 0.02
	55-97.6	0.84 \pm 0.03
+10% mixing water	55-85.1	0.85 \pm 0.03
	55-97.6	0.93 \pm 0.02
-20% mixing water	55-85.1	0.47 \pm 0.03
	55-97.6	0.59 \pm 0.03

4. Numerical modelling of drying of cementitious material

4.1 Modelling framework

The approach for numerical modelling of the drying process relies upon the solution of a single partial differential equation, which represents a non-steady state diffusion process.

Essential assumptions include among others:

- The material is well hydrated, meaning it is not undergoing any further hydration, which might otherwise cause microstructural alterations and induce further self-desiccation.
- Drying is one dimensional and one-faced and the concrete or SLC overlay only exchange moisture with the exterior (not the substrate).

The primary equation (hereafter referred to as Eq. 1) that is solved in this process characterizes the drying phenomenon. The variables required as inputs for solving Eq. 1 are derived using:

- Eq. 2 to Eq. 12 to calculate the gradient (slope) of the sorption isotherm.
- Eq. 14 to calculate the moisture diffusivity.

In terms of boundary conditions, we assume a fixed condition where the external environment remains constant.

To solve Eq. 1, we employ the Crank-Nicolson method. This is an implicit finite-difference technique used for solving time-dependent partial differential equations. The Crank-Nicolson method is known for its second-order accuracy both in time and space, making it a reliable choice for this application. The numerical computation script is provided in Appendix 1.

To summarize, the numerical modelling approach for the drying process involves solving a diffusion-based partial differential equation, using specified inputs and boundary conditions. This approach assumes a well-hydrated material and applies the Crank-Nicolson method to solve the equation.

4.2 Case study

For illustration of the potential application of the numerical modelling framework, a simple case study was undertaken using input data for the SLC product SLC-A investigated by (Anderberg & Wadsö 2004). It is assumed that the product is fully hydrated. Table 5 provides an overview of the geometry, boundary conditions, and target.

Table 5: Description of case.

Geometry	Boundary		Target/requirement (internal) RH (%)
Thickness (mm)	(External) RH (%)	Temperature (°C)	At ¼ depth from exposed surface
40	50	20	75

The parameters used in the models for the sorption isotherm (as per Eq. 8 to Eq. 12) and the moisture diffusivity (outlined in Eq. 14) are deduced from empirical data from (Anderberg & Wadsö 2004) including an estimated value of the non-evaporable water content at saturation (see above), through nonlinear regression techniques, as visualized in Figures 12(a) and 12(b). The fitted parameters for Eq. 8 and Eq. 15 are presented in Table 6. As the mix composition is unknown, the non-evaporable water content at saturation was estimated using data from Mjörnell (1997), who observed a ratio between the non-evaporable water content at 97% and at saturation for mature OPC concrete with a w/c-ratio of 0.7. The black triangle in Figure 12 (a) shows the non-evaporable water content at 100% RH.

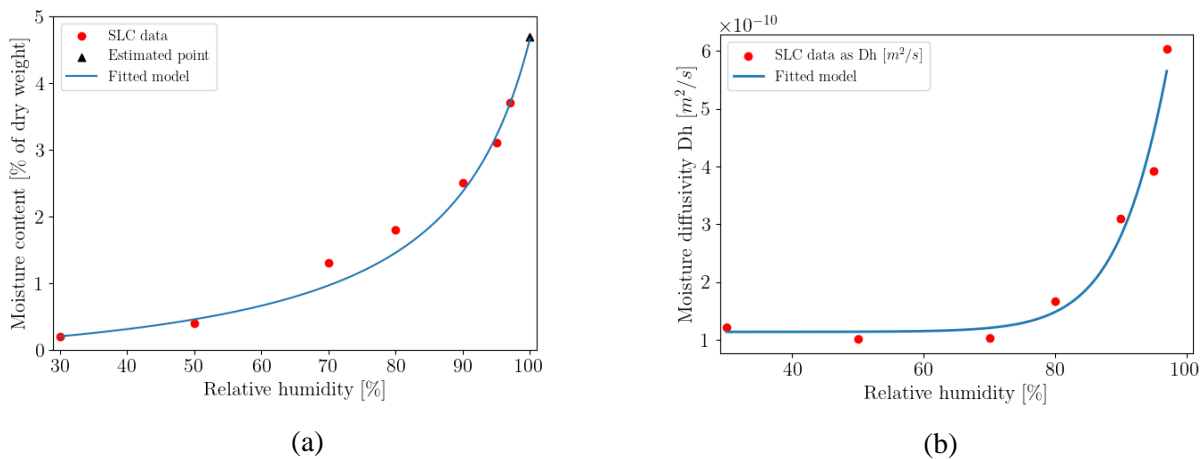


Figure 12: Fitted models (a) Desorption isotherm, data and fitted model using Eq. 8; data from (Anderberg & Wadsö 2004) plus an estimated value of the non-evaporable water content at saturation (black triangle). (b) Moisture diffusivity computed by Eq. 14 using data for total moisture transport coefficients from (Anderberg & Wadsö 2004) and fitted model using Eq. 15.

Table 6: Fitted parameters for Eq. 8 to Eq. 12 describing a desorption isotherm and Eq. 15 and Eq. 16 describing the RH dependend moisture diffusivity obtained by inverse analysis of experimental data in the hygroscopic range $30\% < RH < 97\%$ from Anderberg and Wadsö plus an estimated value of the non-evaporable water content at saturation (see text).

	Moisture diffusivity			Desorption isotherm		
	α_h	β_h	γ_h	k_{wg}	b	$\alpha_C \cdot \zeta_C$
$30\% < RH < 100\%$	1.13e-10	1.30e-9	7.06	9.85e-5	5.21	0.12

As discussed earlier the moisture content (evaporable water content) is measured as percentage of dry weight (i.e., per mass). However, for the numerical modelling approach develop here, the evaporable water content should be represented as kg/m^3 (i.e., per volume). The conversion was made using the following expression:

$$w_e (\text{kg/m}^3) = \frac{\% \text{ of dry weight}(\text{kg/kg}) \times \rho(\text{kg/m}^3)}{100} \quad \text{Eq. 17}$$

Where ρ is the density of material in dry state. According to the supplier the density of the material in saturated state is 1900 kg/m^3 . Using the estimated point of evaporable content at saturation (4.6% of dry weight), the dry density becomes $\frac{1900 \times 100}{104.6} = 1816 \text{ kg/m}^3$. As no information on material composition is available this value was used in Eq. 17.

The time to reach is 75% at $\frac{1}{4}$ of the depth is calculated by solving Eq. 1, while considering external humidity at 50%. In Figure 13, drying profiles for slab is illustrated. This profile is the result of computational simulations. Due to the apparent absence of combined experimental measurements of the drying process and relevant material property data, the simulation outcomes have not yet been tested. Notably, there exists a commercial online tool designed for simulating the drying process (Weber SE 2023). However, this tool does not provide user access to equations and material properties and can thus not be used for verification of the results.

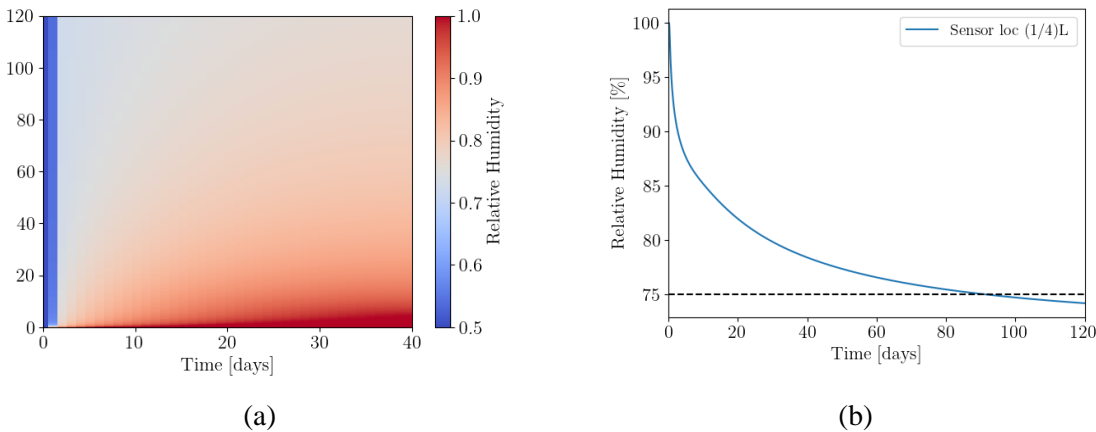


Figure 13: Result of numerical simulation for change in internal RH during one-faced drying of a SLC overlay with thickness of 40 mm. (a) RH as a function of depth from top of slab and time. (b) RH as function of time at the location of $\frac{1}{4}$ of the depth of the slab (sensor location $\frac{1}{4}L$). The horizontal black line indicates the target requirement (75% RH at $\frac{1}{4}$ from the top of the slab/the exposed surface).

5. Sensitivity study

A sensitivity analysis was conducted to illustrate the influence of geometry and boundary conditions on the period of drying before reaching a given target. The scenarios analysed are listed in Table 7. Materials data from the cases study of SLC-A described in Section 4.2 is used.

Table 7: Description of cases for sensitivity study.

Geometry	Boundary conditions		Target/requirement (internal) RH (%)	
	(External) RH (%)	Temperature (°C)	Depth from top $\frac{1}{4}$	Depth from top $\frac{1}{2}$
Thickness (mm) 20, 40, 60	50, 70	20	75	85

The drying patterns at $\frac{1}{4}$ and $\frac{1}{2}$ from the top of the slab/the exposed surface are presented in Figure 14 (sensor location $\frac{1}{4}L$ and $\frac{1}{2}L$, respectively). The simulations highlight the importance of controlling the external relative humidity at the boundary (i.e., constant low RH and circulation to remove moisture and the interface) and the impact of the slab thickness, which might vary over the floor area. From Figure 14 it is noted that the requirement of 85% RH at $\frac{1}{2}$ depth is much more rapidly obtained compared to the requirement of 75% RH at $\frac{1}{4}$ depth (from the top of the slab/the exposed surface).

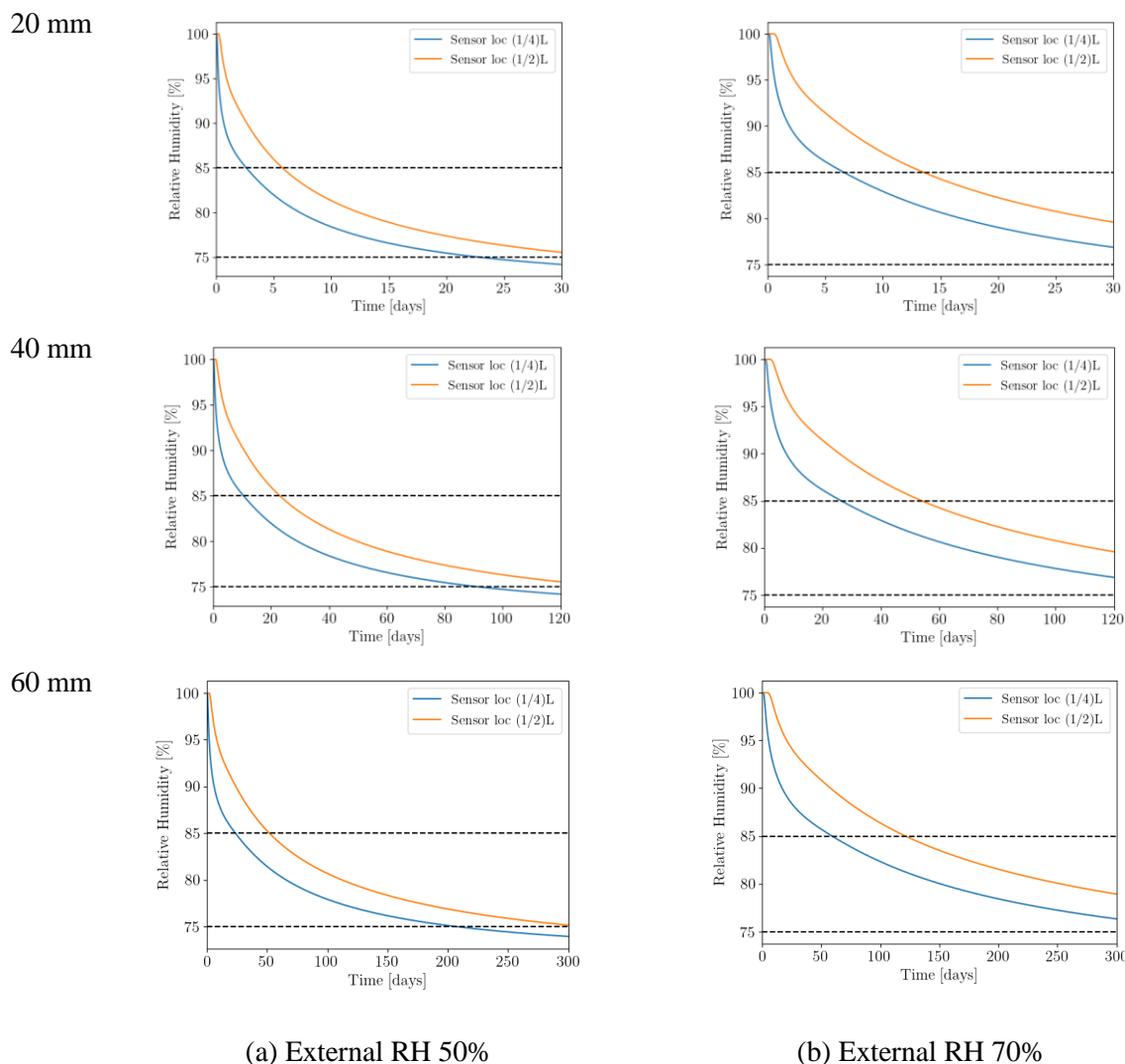


Figure 14: Result of numerical simulation of change in internal RH during one-faced drying of SLC-A overlay with thickness of 20 mm, 40 mm, or 60 mm (top, middle, bottom). (a) External RH set at 50%. (b) External RH set at 70%. The horizontal dotted black lines indicate the two-target requirement of 85% and 75% at $\frac{1}{2}$ and $\frac{1}{4}$ depth from the exposed surface corresponding to sensor location $\frac{1}{2}L$ (orange line) and $\frac{1}{4}L$ (blue line), respectively. Note the difference in time scale (0-30 days, 0-120 days, and 0-300 days) for the three slab thicknesses.

6. Conclusion

Based on literature, a constitutive equation for drying of concrete and key input parameters were identified (addressing Tasks 1.1 and 1.2 of project ICD 521). The key input parameters are the desorption isotherm and the moisture diffusivity, both in the relevant range of relative humidity (75% to 100% RH). Models describing desorption isotherms and moisture diffusivity of concrete were identified. A modelling framework (script) was prepared to allow for numerical modelling of the drying of a (mature) concrete or self-levelling flooring compound. Finally, a sensitivity study was undertaken (addressing Tasks 1.3 of project ICD 521).

The numerical modelling approach for the drying process involves solving a diffusion-based partial differential equation, using specified inputs and boundary conditions. The approach assumes a well-hydrated material and applies the Crank-Nicolson method to solve the equation. Due to the apparent absence of combined experimental measurements of the drying process and relevant material property data, the simulation outcomes have not been tested.

When predicting drying of a material with (partly) unknown composition and properties, assumptions on the desorption isotherm including moisture content at saturation and after self-desiccation, and the moisture diffusivity must be made. To facilitate future drying simulations, it is suggested to establish a database. Available models for desorption isotherms and moisture diffusivity of concrete could be applied to the literature data for a self-levelling flooring compound to provide continuous input data for the drying modelling.

The sensitivity study highlighted the importance of controlling the external relative humidity at the boundary (i.e., constant low RH and circulation to remove moisture on the interface) and the impact of the slab thickness, which might vary over the floor area.

References

- Anderberg, A. & Wadsö, L. (2004a). "Moisture in self-levelling flooring compounds. Part I. Water vapour diffusion coefficients." *Nordic Concrete Research*, 32(2), 3–15.
- Anderberg, A., & Wadsö, L. (2004b). "Moisture in self-levelling flooring compounds. Part II. Sorption isotherms." *Nordic concrete research*, 32(2), 16–30.
- Baroghel-Bouny, V. (2007a). "Water vapour sorption experiments on hardened cementitious materials. Part I: Essential tool for analysis of hygral behaviour and its relation to pore structure." *Cement Concr. Res.*, 37(3), 414–437.
- Baroghel-Bouny, V. (2007b). "Water vapour sorption experiments on hardened cementitious materials. Part II: Essential tool for assessment of transport properties and for durability prediction." *Cement Concr. Res.*, 37(3), 438–454.
- Bažant, Z. P., Krístek, V., and Vitek, J. L. (1992). "Drying and cracking effects in box-girder bridge segment." *J. Struct. Eng.*, 10.1061/(ASCE)0733-9445(1992)118:1(305), 305–321.
- Bažant, Z. P., & Najjar, L. J. (1972). "Nonlinear water diffusion in nonsaturated concrete." *Mater. Struct.*, 5, 3–20.
- Breugel, K. V., & Koenders, E. A. B. (2001). "Numerical simulation of hydration-driven moisture transport in bulk and interface paste in hardening concrete." *Cement Concr. Res.*, 30(12), 1911–1914.
- Brouwers, H.J.H. (2004). "The work of Powers and Brownard revisited: Part 1." *Cement and Concrete Research*, 34(9), 1697-1716.
- Brunauer, S., Emmett, P. H., & Teller, E. (1938). "Adsorption of gases in multimolecular layers." *J. Am. Chem. Soc.*, 60(2), 309–319.
- Brunauer, S., Skalny, J., & Bodor, E. E. (1969). "Adsorption on nonporous solids." *J. Colloid Interface Sci.*, 30(4), 546–552.
- Di Luzio, G., & Cusatis, G. (2009b). "Hygro-thermo-chemical modelling of high-performance concrete. II: Numerical implementation, calibration, and validation." *Cement Concr. Compos.*, 31(5), 309–324.
- Geiker, M. R. (2012). "On the importance of execution for obtaining the designed durability of reinforced concrete structures." *Materials and corrosion - Werkstoffe und Korrosion*, 63(12), 1114-1118.
- Geiker, M. R., Ekstrand, J. P., & Hansen, R. (2007). "Effect of mixing on properties of SCC." In: 5th International Symposium on Self-Compacting Concrete, Ghent.
- Gong, F., Zhang, D., Sicat, E., & Ueda, T. (2014). "Empirical estimation of pore size distribution in cement, mortar, and concrete." *J. Mater. Civ. Eng.*, 26(7), 04014023.
- Havlásek, P. (2014). "Creep and shrinkage of concrete subjected to variable environmental conditions." Ph.D. thesis, CTU in Prague, Prague.
- Huang, Q., Jiang, Z., Gu, X., Zhang, W., & Guo, B. (2015). "Numerical simulation of moisture transport in concrete based on a pore size distribution model." *Cem. Concr. Res.*, 67, 31–43.
- Hooton, R. D., Geiker, M. R., & Bentz, E. C. (2002). "Effects of curing on chloride ingress and implications on service life." *Materials Journal*, 99(2), 201-206.

- Künzel, H. M. (1995). "Simultaneous heat and moisture transport in building components." Ph.D. thesis, Fraunhofer IRB, Stuttgart, Germany.
- Lothenbach, B., Durdzinski, P., & De Weerd, K. (2016). "Thermogravimetric analysis, in A Practical Guide to Microstructural Analysis of Cementitious Materials." CRC Press, p. 540.
- Marek, V., & Vitek, J. L. (2016). "Drying Concrete: Experimental and Numerical Modeling." *J. Materials in Civil Eng.*, 28(9), 04016070.
- Mjörnell, K. (1997). "Moisture Conditions in High Performance Concrete mathematical modelling and measurements." Ph.D. thesis, Sweden.
- Muller, A. C., Scrivener, K. L., Gajewicz, A. M., & McDonald, P. J. (2013a). "Densification of C–S–H measured by 1H NMR relaxometry." *The Journal of Physical Chemistry C*, 117(1), 403–412.
- Muller, A. C. A., Scrivener, K. L., Gajewicz, A. M., & McDonald, P. J. (2013b). "Use of bench-top NMR to measure the density, composition and desorption isotherm of C–S–H in cement paste." *Microporous and Mesoporous Materials*, 178, 99–103.
- Nilsson, L.-O. (2018). "Methods of Measuring Moisture in Building Materials and Structures - State-of-the-Art Report of the RILEM Technical Committee 248-MMB." Springer.
- Oh, B., & Cha, S. W. (2003). "Nonlinear analysis of temperature and moisture distributions in early-age concrete structures based on degree of hydration." *ACI Mater. J.*, 100, 361–370.
- Parrott, L. J. (1988). "Moisture profiles in drying concrete." *Adv. Cement Res.*, 1(3), 164–170.
- Sekki, P., & Karvinen, T. (2017). "Numerical simulation and measurements of drying of Finnish concrete grades." *Energy Procedia*, 132, 729–734.
- Pel, L., Ladman, K. A., & Kaasschieter, E. F. (2002). "Analytic solution for the non-linear drying problem." *Int. J. Heat Mass Transfer*, 45(15), 3173–3180.
- Persson, B. (1997). "Moisture in concrete subjected to different kinds of curing." *Mater. Struct.*, 30(9), 533–544.
- Radjy, F., Sellevold, E.J., & Hansen, K.K. (2003). "Isosteric vapor pressure-temperature data for water sorption in hardened cement paste: enthalpy, entropy and sorption isotherms at different temperatures." Department of Civil Engineering, Technical University of Denmark (BYG-DTU).
- Rangelov, M., & Nassiri, S. (2018). "Empirical time-dependent tortuosity relations for hydrating mortar mixtures based on modified Archie's law." *Constr. Build. Mater.*, 171, 825–838.
- Relling, R.H. (1999). "Coastal Concrete Bridges: Moisture State, Chloride Permeability and Aging Effects, in Structural Engineering." Norwegian University of Science and Technology (NTNU): Trondheim, Norway.
- Sharmilan, S., H. Stang and A. Michel (2023). "Enhancement of a multi-species reactive transport model for cement-based materials under cyclic wetting and drying conditions." *Journal of Building Engineering* 77: 107532.
- Weber, S.E. (2023). MoistureCalc. [online] Available at: <https://www.se.weber/berakningscentralen/fuktberakningsprogrammet-moisturecalc>
- Xi, Y., Bazant, Z. P., Molina, L., & Jennings, H. M. (1994a). "Moisture diffusion in cementitious materials: Adsorption isotherms." *Adv. Cement Based Mater.*, 1(6), 248–257.

Xi, Y., Bažant, Z. P., Molina, L., & Jennings, H. M. (1994b). “Moisture diffusion in cementitious materials: Moisture capacity and diffusivity.” *Adv. Cement Based Mater.*, 1(6), 258–266.

Appendix

Python Script

```
"""
Author: Muhammad Zohaib Sarwar
Code: ODE Solution for Drying of Concrete
Code Version: 1.0
"""

import numpy as np
import matplotlib.pyplot as plt
from scipy.linalg import solve_banded
import matplotlib as mpl
import matplotlib
import sympy as sp

# Parameters
L = 0.08# Length of the concrete (m)
Age=0
T = (120 - Age) * 24 * 3600 # Total simulation time (s)
Nx = 80# Number of spatial points
Nt = 3600*24# Number of time points
dx = L / Nx # Spatial step
dt = T / Nt # Time step

# Constants and functions
alpha_h = 1.13e-10
beta_h = 1.30e-09
gamma_h = 7.06

#***** Diffusivity Fitted*****#

def Dh(h):
    return (alpha_h + beta_h * (1 - np.exp(-np.minimum(10 ** (gamma_h * (h - 1)) * np.log(2), 700))))

def dDh(h):
    return (beta_h * gamma_h * 10 ** (gamma_h * (h - 1)) * np.log(10) * np.exp(-np.minimum(10 ** (gamma_h * (h - 1)) * np.log(2), 700)))

#***** Desorption Isotherm*****#
# Symbolic version for differentiation
def desorption_sym(h, k_wg, b, alpha):
    C = 2400
    W_cs = 0.063 * C
    W_o = 1.0 * C
    W_n = C * alpha * 10
    W_tot = W_o - 0.75 * W_n - W_cs
    W_gel = k_wg * alpha * C
    value = (1 - (1 / sp.exp((b - alpha * 10))))
    value2 = (sp.exp((b - alpha * 10)) - 1)
    W_cap = (W_tot - W_gel * value) / value2
```

```

def W_g(h):
    var = (1 / sp.exp((b - alpha * 10) * h))
    return W_gel * (1 - var)

def W_c(h):
    var = (sp.exp((b - alpha * 10) * h) - 1)
    return W_cap * var

    return W_g(h) + W_c(h)
# Fitted Parameter for Equation
k_wg = 8.85e-05
b = 5.24
alpha = 0.12

h_sym = sp.Symbol('h')
u_sympy = desorption_sym(h_sym, k_wg, b, alpha)

#*****Derivative First and Second*****
dSI = sp.diff(u_sympy, h_sym)
ddSI= sp.diff(dSI, h_sym)

dSI_func = sp.lambdify(h_sym, dSI, "numpy")
ddSI_func= sp.lambdify(h_sym, ddSI, "numpy")

def external_humidity(t):
    # Example: sinusoidal variation of external humidity
    h_en_base = 0.65
    amplitude = 0.2
    period = 24* 3600 # 24 hours
    return h_en_base + amplitude * np.sin(2 * np.pi * t / period)

# Initial condition
h0 = 1.0
h1 = 0.6
# Initialize variables and arrays
h_old = np.ones(Nx) * h0
h_new = np.ones(Nx) * h1
A_diag = np.zeros(Nx - 2)
B_diag = np.zeros(Nx - 2)
C_diag = np.zeros(Nx - 2)
RHS = np.zeros(Nx - 2)
h_out=[]

for t in range(int(Age * 24 * 3600 // dt), Nt):
    h_en = external_humidity(t * dt)
    h_en =0.5

# Space loop

```

```

for i in range(1, Nx - 1):
    dSI_h = dSI_func(h_old[i])/18.16    #according to Eq.17
    Dh_h = Dh(h_old[i])
    dDh_h = dDh(h_old[i])
    ddSI_h = ddSI_func(h_old[i])/18.16 #according to Eq.17

    A_diag[i - 1] = -0.5 * dt * Dh_h / (dx ** 2 * dSI_h)
    B_diag[i - 1] = 1 + dt * Dh_h / (dx ** 2 * dSI_h)
    C_diag[i - 1] = A_diag[i - 1]

    RHS[i - 1] = h_old[i] + 0.5 * dt * (Dh_h * (h_old[i + 1] - 2 * h_old[i] + h_old[i - 1]) / (dx ** 2 * dSI_h) -
dDh_h * (h_old[i + 1] - h_old[i - 1]) / (2 * dx) + dDh_h * (h_old[i + 1] - h_old[i - 1]) / (2 * dx))

# Update boundary condition
RHS[0] -= A_diag[0] * h_en # Using the Dirichlet boundary condition
RHS[-1] -= C_diag[-1] * h_en# Using the Dirichlet boundary condition

# Solve the linear system
h_new[1:-1] = solve_banded((1, 1), np.array([C_diag, B_diag, A_diag]), RHS)

h_new[0] = h_en #Fixed boundary condition
h_new[-1] = h_en # Fixed boundary condition

# Update h_old
h_old = np.copy(h_new)
h_out.append(h_old)
cond=2
# Plot results at specific time intervals

if t % (Nt // 15) == 0:
    plt.figure(98)
    plt.plot(np.linspace(0, L, Nx), h_new, label=f"{t*dt/(24*3600):.0f} days")

# Configure and display the plot after the time loop
plt.xlabel(" Position [days]")
plt.ylabel("Relative Humidity [$\%$] ")
# plt.title("Relative Humidity Profile at Different Times")
plt.xlim(0.0, L/2)
plt.legend()
plt.show()
## Convert the output to a 2D array
h_out = np.array(h_out)

#Create a 2D plot
plt.figure(2)
fig, ax = plt.subplots()
X, Y = np.meshgrid(np.linspace(0, L, Nx), np.linspace(Age, T / (24 * 3600), Nt - int(Age * 24 * 3600 //
dt)))
c = ax.pcolormesh(X*1e3, Y, h_out, cmap='coolwarm', shading='auto')
fig.colorbar(c, ax=ax, label='Relative Humidity')

```

```
ax.set_xlabel("Position [mm]")
plt.xlabel("Time [days]")

# ax.set_title("Relative Humidity Profile over Time and Space")
ax.set_xlim(0.0, (L/2)*1e3)
plt.tight_layout()
plt.show()
```

